



Human brain dynamics are shaped by rare long-range connections over and above cortical geometry

Jakub Vohryzek^{a,b,1}, Yonatan Sanz-Perl^a, Morten L. Kringelbach^{b,c,d} , and Gustavo Deco^{a,e} 

Affiliations are included on p. 8.

Edited by Peter Strick, University of Pittsburgh Brain Institute, Pittsburgh, PA; received July 26, 2024; accepted November 10, 2024

A fundamental topological principle is that the container always shapes the content. In neuroscience, this translates into how the brain anatomy shapes brain dynamics. From neuroanatomy, the topology of the mammalian brain can be approximated by local connectivity, accurately described by an exponential distance rule (EDR). The compact, folded geometry of the cortex is shaped by this local connectivity, and the geometric harmonic modes can reconstruct much of the functional dynamics. However, this ignores the fundamental role of the rare long-range (LR) cortical connections, crucial for improving information processing in the mammalian brain, but not captured by local cortical folding and geometry. Here, we show the superiority of harmonic modes combining rare LR connectivity with EDR (EDR+LR) in capturing functional dynamics (specifically LR functional connectivity and task-evoked brain activity) compared to geometry and EDR representations. Importantly, the orchestration of dynamics is carried out by a more efficient manifold made up of a low number of fundamental EDR+LR modes. Our results show the importance of rare LR connectivity for capturing the complexity of functional brain activity through a low-dimensional manifold shaped by fundamental EDR+LR modes.

structure–function | brain connectivity | brain geometry | fMRI | harmonic decomposition

How the underlying anatomy of the brain shapes functional dynamics is an unresolved question being studied from the perspective of network neuroscience (1), brain modeling (2), graph signal theory (3), and neural field theories with different assumptions on the underlying anatomy (4, 5). Therefore, the choice of underlying anatomical features is of paramount importance in deriving the most simple and parsimonious description of the emerging spatiotemporal brain dynamics.

In previous work on retrograde tract tracing in nonhuman primates, Kennedy et al. have shown that the brain white-matter wiring can be analytically approximated by the exponential distance rule (EDR) (6). This rule explains the local connectivity of the brain solely in terms of the Euclidean distance between points on the cortical surface. And so, it follows that the compact, folded geometry of the cortex with its many sulci and gyri is formed by this local connectivity. This corollary implies that the brain anatomical wiring and cortical geometry are the two sides of the same coin, and it makes sense to speak of them in agreement. Furthermore, this reflects theoretical work showing that the heat kernel (exponential) is the optimal solution for minimizing distance between neighboring points (7). Indeed, recent work has suggested that the cortical geometry alone (as a proxy for the underlying anatomical connectivity) can be considered as an important feature driving brain spatiotemporal activity (5, 8, 9).

However, after deriving the EDR Henry Kennedy famously said; “I am not interested in the EDR itself but mainly the exceptions to the rule.” Indeed, Kennedy et al. have shown that in addition to the EDR, the brain possesses a small subset of rare long-range (LR) exceptions to the EDR of brain wiring (10, 11). Furthermore, new evidence using turbulence has demonstrated the fundamental role of the rare LR anatomical connections in shaping optimal brain information processing (12). Intuitively, brain cortical foldings defined according to the EDR are indeed the optimal way for brain wiring but they do not reflect the rare LR connections, i.e., it is, for example, impossible to fold anterior–posterior brain regions in a meaningful way. Therefore, we suggest that the unique contribution of these rare LR cortical connections’ changes disproportionately the topological structure of the brain wiring in such a way as to optimize the information processing of the brain. In this work, we test this hypothesis that EDR and LR exceptions are fundamental to the parsimonious description of the emerging spatiotemporal dynamics.

In the natural world, a fundamental principle that governs the dynamics of a system constrained by its structure in numerous physical and biological phenomena is the

Significance

Explaining how structure of the brain gives rise to its emerging dynamics is a primary pursuit in neuroscience. We describe a fundamental anatomical constraint that emphasizes the key role of rare long-range (LR) connections in explaining functional organization of the brain in terms of spontaneous and task-evoked activity. Specifically, this constraint unifies brain geometry and local connectivity through the exponential distance rule while considering the LR exceptions to this local connectivity as derived from the structural connectome. In addition, when using this structural information, we show that the task-evoked brain activity is described by a low-dimensional manifold of several modes, suggesting that less is more for the efficient information processing in the brain.

Author contributions: J.V., M.L.K., and G.D. designed research; J.V. and Y.S.-P. performed research; J.V. and G.D. contributed new analytic tools; J.V., Y.S.-P., and G.D. analyzed data; and J.V. and M.L.K. wrote the paper.

The authors declare no competing interest.

This article is a PNAS Direct Submission.

Copyright © 2025 the Author(s). Published by PNAS. This article is distributed under [Creative Commons Attribution-NonCommercial-NoDerivatives License 4.0 \(CC BY-NC-ND\)](https://creativecommons.org/licenses/by-nc-nd/4.0/).

¹To whom correspondence may be addressed. Email: jakub.vohryzek@upf.edu.

This article contains supporting information online at <https://www.pnas.org/lookup/suppl/doi:10.1073/pnas.2415102122/-/DCSupplemental>.

Published January 3, 2025.

mathematical framework of harmonic modes. Standing wave patterns manifest in many contexts such as in music with sound-induced vibrations of a guitar string, in physics with the electron wave function of a free particle described by the time-independent Schrödinger equation, or biology with patterns emerging within complex dynamical systems like reaction–diffusion model (13). The relevance of the mathematical formalism of this phenomenon is that it links in a single equation, the Helmholtz equation, the specific structure on which the spatiotemporal pattern emerges together with the temporal description in terms of oscillations and spatial description in terms of patterns of synchrony of the standing wave pattern itself.

Here, we used Laplacian decomposition of four different graph representations of the underlying anatomy to derive anatomical brain modes: EDR (6) and LR exceptions (EDR+LR), geometry-based modes (geometry), and EDR modes (EDR binary and EDR continuous) (Fig. 1 *A–C*). Our results show that EDR+LR achieves statistically better reconstruction of LR functional connectivity (FC) compared to the other mode representations (Fig. 1*D*). Furthermore, pertinent to time-critical information processing, we show that a small subset of modes achieves a disproportionately high reconstruction of task-activation (TA) brain maps. When this subset of modes is considered, EDR+LR achieves better reconstruction for the 47 HCP tasks compared to the geometric mode representations, suggesting that less is more for information processing in the brain (Fig. 1*E*).

Results

EDR+LR Reconstructs FC LR Connectivity. To examine how EDR with LR exceptions can describe brain activity, we derived the EDR+LR harmonic modes from the EDR matrix fitted to the structural connectome with λ of 0.162 and added the LR exceptions to the EDR defined in terms of three SD from a given Euclidean distance range larger than 40 mm. We constructed the normalized graph Laplacian and solved its eigenvalue problem (Fig. 1*B*). The eigenvectors of the solution represent the harmonic modes with the eigenvalues sorted in ascending order and reflecting the spatial frequency of the modes with lower modes representing lower spatial frequencies and higher modes representing higher spatial frequencies. Overall, the spatiotemporal activity can be perceived as a weighted contribution of these fundamental bases unfolding over the whole time recording for the spontaneous fMRI or as a weighted contribution of these fundamental bases reconstructing the task-based activations brain maps.

One of the features of FC is the surprisingly high FC between distant regions (14). We first investigated to what extent the different anatomical representations reconstruct the LR connections. These were derived as an intersection of FC connections above 0.5 FC correlations and Euclidean distance between the nodes above 40 mm (Fig. 2*A*). We then reconstructed these connectivity profiles with an increasing number of modes (1 to 200) derived from the four representative graphs (geometry, EDR binary, EDR continuous, and EDR+LR) (Fig. 2*B*). The modes are ordered sequentially according to their spatial wavelength represented by their eigenvalues (i.e., mode 1 has the longest spatial wavelength). For all four graphs, they monotonically decrease the reconstruction distance reaching on average 0.03 mse distance with about 20 modes and by 100 modes reach on average 0.01 mse distance before plateauing close to 0.005 mse distance on average for the full 200 modes. One noteworthy aspect is that much of the distance reconstruction happens between 1 and 20 harmonics suggesting that a small number of harmonics is responsible for most of the reconstruction. At 200 modes the EDR+LR outperforms

the other spatial basis (geometry, EDR continuous, EDR binary, paired t test $P < 10^{-4}$). To assess the uniqueness of the LR connections within the EDR graph, we created a null model where we shuffled the LR connections in the EDR+LR graph representation. As expected, the specific rare LR connectivity is important since the shuffled EDR+LR modes were unable to reconstruct the LR FC to the same extent as the EDR+LR (SI Appendix, Fig. S4). Furthermore, to assess whether the EDR+LR performance is due to the unique combination of EDR and LR connectivity, we computed the reconstruction when using the structural connectome that implicitly contains the short-range and LR connectivity and LR connectivity exceptions. However, as expected, the structural connectome graph representation showed less reconstruction capacity in comparison to the other representations (SI Appendix, Fig. S5). Finally, to ensure robustness of the result, we carried out the analysis on an additional subset of 100 HCP participants reporting the same statistical significance between EDR+LR and geometry (SI Appendix, Fig. S11).

Less Is More: EDR+LR Reconstructs Task Activations with Fewer Modes. Using the same approach, we further investigated how well the different bases reconstruct the task-evoked brain activity from 255 healthy HCP participants. We used the 47 task-based contrasts derived from 7 HCP tasks each representing a different task-activation brain map and reconstructed them for an increasing number of modes (mode 1 to 200). For the seven representative tasks, the different bases demonstrate a similar monotonic pattern with steep fall in reconstructed mse distance before a slowdown with a near plateau-like behavior around 200 modes and reconstructed mse distance values approximating 0.02 for most of the bases and tasks (Fig. 3 *A, Top*). To analyze the reconstruction pattern, we computed the TA mse contribution of a given mode when added to the reconstruction. This demonstrates that the apparent bulk of the reconstruction is being obtained from a relatively small number of modes 1 to 20 in comparison to the rest (Fig. 3 *A, Bottom*). This shows that reconstructing both spontaneous and task-evoked activity is represented in a very small space of 1 to 20 modes, suggesting that both types of dynamics, spontaneous and task-evoked, lie in a lower-dimensional manifold. Focusing only on the first 20 modes, we examined how the 47 task-evoked activations maps are reconstructed in comparison to the geometric modes. On average EDR+LR compared to geometry shows the most accurate reconstruction across tasks up to 20 reconstructed modes (Fig. 3*B*). By construction, the modes span an orthogonal basis set in which the individual mode contributions are mapped to. To motivate the neatness and accuracy of reconstructing the task-activation maps with as little EDR+LR as possible, we visually demonstrate the reconstruction of relational tasks for 5, 10, 15, and 20 modes showing the indistinguishable similarity to the activation map itself (Fig. 3*C*). Moreover, it is not surprising that the EDR+LR basis, due to their unique topology, reconstructs with fewer modes more accurately the tasks as it can be appreciated in the motor tasks where more nuanced features are picked up in comparison to the geometric modes (Fig. 3*D*).

Discussion

The unique mathematical formulation of harmonic modes links the description of how structure gives rise to the emerging spatiotemporal activity of brain dynamics. We show that EDR+LR modes have the smallest reconstruction distance for an increasing number of modes when describing the FC LR connections of spontaneous fMRI activity. Furthermore, for the reconstruction of the seven activation task fMRI maps lower frequency modes

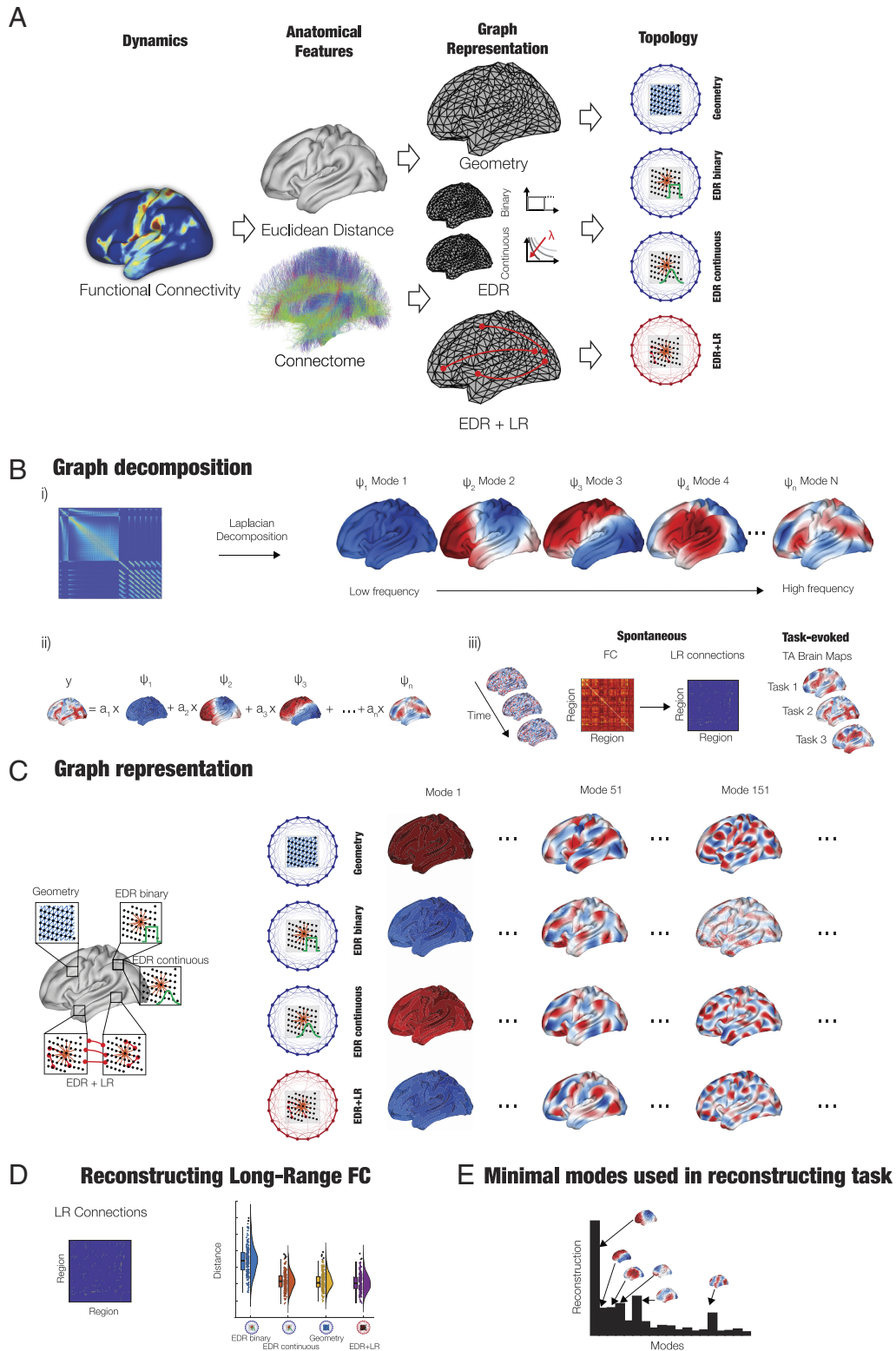
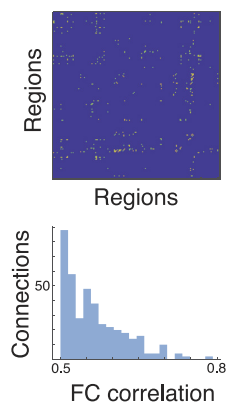
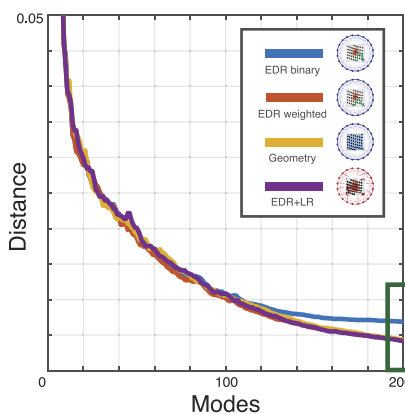


Fig. 1. The crucial role of LR connectivity for accurately describing whole-brain dynamics. (A) The functional dynamics measured with fMRI emerge from the underlying anatomical structural connectivity which can be represented as graphs. Here, we study the four main graph representations: 1) geometrical modes (5); 2) EDR (binarized); 3) EDR (continuous); and 4) EDR with LR exceptions (EDR+LR). (B) With regard to the graph representations, i) the different modes are derived from applying the Laplace decomposition on the graph representation by solving the eigenvalue problem. The different modes are in ascending spatial frequency. ii) These modes are used to reconstruct the fMRI activity by a linear combination of their contributions. iii) This is used to reconstruct the spontaneous fMRI activity, and particularly the functional LR connectivity exceptions (derived as high-correlation values, >0.5 correlation, and over a long Euclidean distance, >40 mm, see *Materials and Methods*), as well as all the 47 task-activation brain maps. (C) The four different graph representations were constructed and decomposed into their associated modes. (D) Demonstrating the importance of LR connections, EDR+LR achieves a superior reconstruction of LR fMRI connectivity compared to geometric, EDR (binary), and EDR (continuous) graph representations. (E) Equally important, the EDR+LR needs fewer modes to reconstruct task data compared to the three other graph representations, demonstrating the importance of LR connectivity. Parts of the figure have been modified from work by Pang et al. (5).

A FC long-range exceptions



B Reconstruction accuracy



C Reconstruction for 200 modes

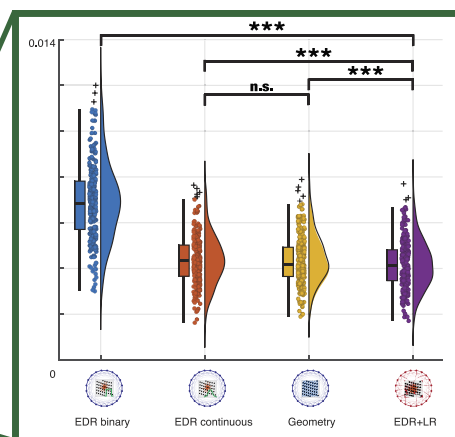


Fig. 2. Better reconstructions of brain dynamics are found with EDR and rare LR exceptions in the graph representation. (A) One of the most important features of cortical dynamics are LR functional connections (defined by high correlation values, >0.5 correlation, and Euclidean distance, >40 mm). (B) The reconstruction of FC LR connections for an increasing number of modes (1 to 200) for the four representative graph representations. The individual lines show the average across all 255 HCP participants. (C) EDR+LR is significantly better than the other graph representations when using a reconstruction with 200 modes as shown by the average result for the distance values across all the 255 HCP subjects (Bonferroni-corrected two-tailed paired t test, EDR+LR and geometry $P < 0.0005$, EDR+LR and EDR continuous $P < 10^{-4}$, EDR+LR and EDR binary $P < 10^{-4}$, and EDR continuous and geometry n.s., * $P < 0.05$, ** $P < 0.01$, and *** $P < 0.001$).

contribute disproportionately more toward the reconstruction error. We therefore reconstructed the error for the 47 HCP tasks benchmarked against the geometrical modes for the first 20 modes. On average, EDR+LR showed the most accurate reconstruction across tasks and number of reconstructed modes 1 to 20. Our results demonstrate the importance of LR connectivity as a key feature of shaping brain functional activity both for the spontaneous and task-based fMRI. Moreover, functional brain activity is shown to be on a lower-dimensional manifold span by a subset of these fundamental modes with the most appropriate representation from the EDR+LR graph, suggesting that less is more for efficient information processing in the brain.

In both spontaneous and task-based reconstruction cases, the EDR+LR demonstrates high reconstruction only with a subset of modes from its harmonic repertoire. Despite the overall better performance of the EDR+LR harmonic modes, it is remarkable that the other harmonic bases, geometric and EDR-based, performed strongly as well. This excellence can be seen from the fact that all four reconstruction schemes are able to predict behavioral measures fluid intelligence and participant's processing speed. The results show that this prediction is driven by the brain state (task-evoked over spontaneous fMRI) consistently across the four graph representations (*SI Appendix, Figs. S6–S8*). This reflects a fundamental insight where large-scale brain organization can be described as lying in a low-dimensional manifold. This in part can be explained by the brain's coordinated cognition and behavior which cannot happen without integrative tendencies of its underlying dynamics. Indeed, brain dynamics operating in a reduced number of dimensions have been shown to predict more effectively the brain's behavior (15). As such one can talk of brain activity as a flow on this low-dimensional manifold embedded in the space of these relatively few harmonic modes (16).

One of the fundamental considerations is what type of brain's dynamics we wish to reconstruct. Unlike the traditional approach where the whole static FC is reconstructed (5), we focused on reconstructing the most salient features of the brain's spontaneous fMRI activity, namely the functionally strong LR connections. Our work underscores the cardinal role of LR connectivity in cognitive processing and advocates for prioritizing the reconstruction of exceptional connections over exhaustive coverage of the entire FC matrix.

With similar logic, we did not regress out the global signal from the spontaneous fMRI as we consider the global and fluctuating fMRI activity an important feature of emergent network effects of interacting nonlinear regional dynamics (17). As expected, when we computed the analysis, applying global signal regression, the reconstruction of EDR+LR and geometry were statistically nonsignificant (*SI Appendix, Fig. S9*). Moving beyond, it is important to consider temporally evolving descriptions of brain dynamics as recent work has demonstrated the relevance of dynamics in understanding brain function and its related pathologies (18). Also, many whole-brain modeling techniques have been suggesting the need to consider further descriptors of brain activity that goes beyond the static FC description (19). Ultimately, as recently suggested by the spatiotemporal neuroscience of Northoff et al. (20, 21), the brain's dynamic spatiotemporal organization might reveal the link between the neuronal and mental features to elucidate concepts such as consciousness, self, and time speed perception.

Flexible human cognition and behavior reflect a highly dynamic balance of functional integration and segregation. This in turn is supported by the rich topology of the structural connectome (22). A growing body of literature has shown that these dynamics are poised at the edge of criticality, a dynamic regime with LR spatial and temporal correlations in which information can be optimally processed (19). This is consistent with a novel computational framework by Jaeger et al. (23), suggesting that an understanding of computing comes from an understanding of the structuring of processes, rather than how classical models of computing systems describe the processing of structures. They also stress how this can come via an understanding of modeling physical computing systems bottom-up, which is the main aim of the investigation here, where the topology of the computing system, here the brain, shapes the near-critical dynamics of the system. In the brain, the rare LR structural connections are some of the key anatomical features supporting time-critical information processing. Their spatially specific location has been linked to the emergence of known resting-state networks and are important for task-based processing (12). We therefore hypothesize that evolutionary pressures are likely to have refined EDR connectivity with LR exceptions enabling more complex cognitive functions. This hypothesis should be investigated in future cross-species studies.

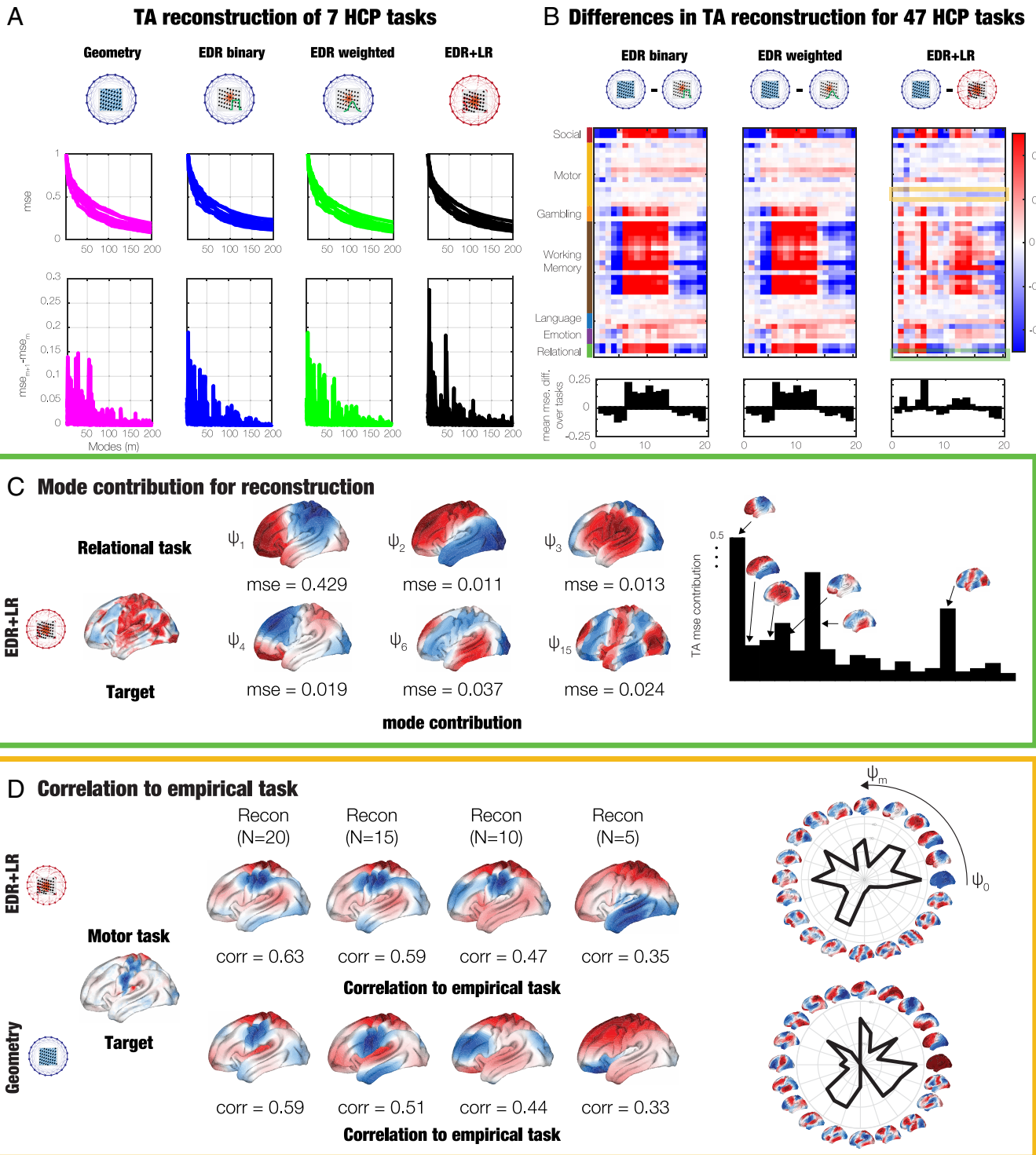


Fig. 3. EDR+LR uses fewest harmonic modes to reconstruct task activity. (A) For each of the four graph representations (*Top panel*) the reconstruction of seven representative task- activation maps is shown in terms of normalized mse distance (distance normalized by the max of each task). As can be seen, lower frequency modes contribute disproportionately more toward the reconstruction distance as it can be seen by the elbow around 20 modes (*Lower panel*). (B) This can also be seen in the reconstruction mse distance for all 47 HCP tasks for the EDR+LR, EDR binary, and EDR continuous, each benchmarked against the geometrical modes for the first 20 modes, where the *Top panel* shows hues of blue with better performance of the EDR modes while red hues mean better performance of the geometric modes. The *Lower panel* shows the average across the 47 HCP tasks. (C) Individual mode contribution toward the reconstruction of the relational task. We show the disproportional contribution of some modes (1–4, 6, 15) to the overall reconstruction, where the brain renderings show the mse distance reconstruction to the overall task-activation map (*Far Left*). (D) Similarly, for the motor task target (*Far Left*), we compare the overall correlational contributions of the number of modes (using 20, 15, 10, and 5 modes) when using EDR+LR and geometry as the underlying representations. As can be seen, the reconstruction with EDR+LR converges more quickly for lower modes than geometry.

In this work, we derived both EDR binary and EDR continuous harmonic modes. These reflect different methodological considerations when calculating the Laplacian eigenmaps (7). We have applied the continuous form of the graph Laplacian on the EDR

(EDR continuous) showing that this simple change improves the reconstruction accuracy by about 0.0025 distance to the binarized version (EDR binary) making it practically on the same footing as the geometric bases (EDR continuous and geometry are not

statistically different from each other). Reassuringly, recent work has reported similar observations when comparing the nonbinarized structural connectomes graph representation to the geometric modes (24). It is therefore warranted to unify the methodological approaches before comparing the superiority of the different anatomical features as the differences might be simply explained by methodological choices themselves. Therefore, we caution future research to unify the applied methodologies in this direction.

Given the relevance of rare LR connectivity for complex brain dynamics in humans, it is also important to consider how these findings might translate to other nonhuman species. Unfortunately, a direct comparison between species is challenging due to the different methodologies used. Unlike nonhuman species studies that use track tracing studies to describe the anatomical connectivity of the brain, human experiments rely on noninvasive techniques like diffusion MRI. Furthermore, the challenges in estimating LR connectivity via dMRI further complicate the direct comparison (25, 26). Yet, a growing body of nonhuman species studies have converged on a general principle that smaller brains such as the mice brain are denser, all-to-all connected, whereas larger brains such as the primate brains are sparser with weak LR connections reflecting further regional specialization (27, 28). Therefore, it can be hypothesized that LR EDR connections together with the rare connectivity exceptions play an important role in the emergence of complex computational capabilities. This opens up exciting future cross-species research of the impact of rare LR connections on the brain's computational capabilities.

Understanding rare LR connections' impact on the emergent brain dynamics will also help clinical diagnosis in neuropsychiatry and neurology, and inform more accurate clinical treatments. For instance, the weak nature of these rare LR connections might be abnormally affected in disconnection syndromes such as Alzheimer's disease and schizophrenia, and this in turn might have a disproportionate impact on the large-scale emergent dynamics affecting cognition and behavior (27). Moreover, novel treatment solutions, such as transcranial electrical stimulation, will rely on model optimization where anatomical connectivity plays an important role (29, 30). In the future, the specific inclusion of rare LR connections in the models might ensure more accurate description of the disorders as well as more efficient stimulation protocol for possible treatments.

Materials and Methods

Experimental Data.

HCP functional MRI. We utilized the publicly available Human Connectome Project (HCP) dataset, Principal Investigators: David Van Essen and Kamil Ugurbil: 1U54MH091657) with the funding coming from sixteen NIH Institutes and Centers supporting the NIH Blueprint for Neuroscience Research; and by the McDonnell Centre for Systems Neuroscience at Washington University. All participants joined voluntarily and provided informed consent. The open-access data used in this study were obtained through the WU-Minn HCP consortium, following approval from the local ethics committee. The data were shared with the authors in accordance with the terms specified by the HCP for data usage. All procedures conducted in this study adhered to the protocols outlined in these data use terms. For a comprehensive description of the image acquisition protocol, preprocessing pipelines (31), and ethics oversight, please refer to the detailed account provided (31, 32).

Spontaneous fMRI dataset. We used the spontaneous fMRI dataset from the freely accessible database with connectome DB account at <https://db.humanconnectome.org>. Time series were minimally processed. Consistent with work of Pang et al. (5), we used a subset of 255 participants (22 to 35 y old, 132 F and 123 M) who completed all spontaneous and tasks-based fMRI recordings, further excluding twins and siblings. For the auxiliary dataset, we used a subset of 100 HCP participants which were different to the main analysis performed with the 255 HCP participants. The neuroimaging acquisition was

carried out on a 3-T connectome-Skyra scanner (Siemens). A single spontaneous fMRI acquisition, lasting approximately 15 min, was conducted on the same day. During this session, participants kept their eyes open with relaxed fixation on a projected bright crosshair against a dark background. The HCP website offers comprehensive details on participant information, acquisition protocols, and data preprocessing for both spontaneous and the seven tasks. In summary, the data underwent preprocessing using the HCP pipeline, which employs standardized methods with FSL (FMRIB Software Library), FreeSurfer, and Connectome Workbench software. This standardized preprocessing encompassed correction for spatial and gradient distortions, head motion correction, intensity normalization, bias field removal, registration to the T1-weighted structural image, transformation to the 2-mm MNI space, and application of the FIX artifact removal procedure. Head motion parameters were regressed out, and structured artifacts were removed using independent component analysis, followed by FMRIB's ICA-based X-noiseifier (ICA+FIX) processing. The preprocessed time series for all grayordinates were in the HCP CIFTI grayordinates standard space, available in the surface-based CIFTI file for each participant during spontaneous fMRI. Finally, for *SI Appendix, Fig. S9*, we also regressed out the global signal before carrying on with further analysis on the spontaneous fMRI.

Tasks-based fMRI dataset. For the task-based fMRI analysis, we obtained fMRI data from seven distinct task domains known to reliably engage a diverse range of neural systems (5, 31). The tasks included were social, motor, gambling, working memory, language, emotion, and relational. We used the specific contrasts within each task domain, highlighting the key contrast investigated in this study. These contrasts were provided by work of Pang et al. (5) from <https://osf.io/xczmp/> in "S255_fmri_ALLTASKS_raw_lh" .mat file. In total, the analysis encompassed 47 contrasts, incorporating the seven key contrasts. In brief, the analysis was performed on individual task-activation maps generated through FSL's cross-run (Level 2) FEAT analysis (33). The task maps, provided by the HCP, were used with minimal smoothing (2 mm), and mapped onto the fsLR-32 k CIFTI space. This mapping was achieved using multimodal surface matching, resulting in a representation of each individual's task data (32,492 vertices). Additional information about each task and contrast as well as further details on the data are provided elsewhere (5, 31). The task-evoked fMRI reconstruction distance was computed on the parcellated activation maps, unlike those using spontaneous fMRI, where the reconstruction distance was performed on the parcellated functional LR connections.

fMRI parcellation. A custom MATLAB script, utilizing the "ft_read_cifti" function from the Fieldtrip toolbox, was employed to extract the average time series of all grayordinates in each region defined by the Glasser360 parcellations (180 regions per hemisphere) in the HCP CIFTI grayordinates standard space. For each hemisphere, the vertex-space to ROI-space meant going from $32,492 \times 1,200$ to $180 \times 1,200$ for spontaneous fMRI and $32,492 \times 1$ to 180×1 for task-based fMRI. Consistent with work by Pang et al. (5), our analysis focused on the left hemisphere only.

HCP diffusion MRI. To obtain the structural connectivity for the fitting of the EDR and derivation of LR exceptions to the EDR, we used the high-resolution connectivity maps from dMRI tractography (34). These were provided by work of Pang et al. (5) in "S255_high-resolution_group_average_connectome_cortex_nomedial-lh" .mat file. In brief, the connectome was derived by estimating the connectivity of each of the 32,492 vertices within the cortical surface mesh by tracing streamlines from each point until they terminated at another point. Connection weights between vertices, treated as nodes, were determined as the number of interconnecting streamlines without normalization (35). The dMRI tractography was conducted on individuals from the HCP. Subsequently, the individual weighted connectivity matrices were combined, each of size $32,492 \times 32,492$, to generate a group-averaged connectome. The weights in this connectome represented the average number of streamlines, providing a comprehensive depiction of group-level connectivity. Further details can be found in previous publication by Pang et al. (5).

Structural MRI. For the fitting of the EDR, we used the Euclidean distance between the vertices of the cortical mesh representation for the left hemisphere ($32,492 \times 32,492$). This mesh was derived from the FreeSurfer's fsaverage population-averaged template available on github.com/ThomasYeoLab/CBIG/tree/master/data/templates/surface/fs_LR_32k. It is to be noted, we used the version provided by Pang et al. (5) in the "fsLR_32k_midthickness-lh" .vtk file.

EDR. Previous work has demonstrated that the brain white-matter wiring, based on retrograde tract tracing in nonhuman primates, can be analytically approximated by the EDR (6). Here, we derived the EDR of the underlying human anatomy using diffusion MRI (SI Appendix, Fig. S3). Mathematically, the EDR can be described with exponential decay function as follows:

$$C_{ij}^{\text{EDR}} = Ae^{-\lambda r(i,j)},$$

where $r(i, j)$ is the Euclidean distance between vertices i and j and λ is the decay. Consistent with previous literature, we estimated the parameters (A and λ) for the exponential decay model using a least-squares method as follows $y = Ae^{-\lambda x}$, where y represents a mean connection weight of a given Euclidean distance and x represents the given Euclidean distance (12). In detail, we have generated 400 bins of equal Euclidean distance taking the bins spanning 10 to 170 mm (thus excluding the first 25 bins in the fitting procedure). The estimation yielded $A = 0.066$ and $\lambda = 0.162 \text{ mm}^{-1}$ where the exponential decay parameter λ is consistent with previous literature (10, 12). We used this estimation for the construction of the EDR+LR graph. For the EDR binary and EDR continuous, we used previously reported exponential decay parameter of $\lambda = 0.12 \text{ mm}^{-1}$ to be consistent with work of Pang et al. (5) (EDR Binary and EDR Sontinuous).

Relationship to belkin and niyogi. The EDR, as an optimal solution for connecting distance-separated brain regions in the brain, can also be intuitively understood from first principles. Belkin et al. have analytically shown the relationship between graph Laplacian, Laplace-Beltrami operator, and the heat kernel which is the

optimal solution for locality preservation - formally as $W_{ij} = e^{-\frac{\|x_i - x_j\|^2}{t}}$ where t is the decay parameter of the heat kernel (7). It can thus be appreciated that this equation also follows exponential decay (Gaussian) similar to the EDR.

Harmonic modes. In this work, we used four different types of graph representations to describe various aspects of anatomical features or methodological approaches. Namely, we carried out the analysis on what we call Geometric, EDR binary, EDR continuous and EDR+LR modes. In what follows, we describe the remaining three types of harmonic modes representations.

EDR binary. For the EDR binary, we use the EDR with the same parameters as in work of Pang et al. (5) to define the weight of a given edge between vertices i and j . In other words, the weight is determined by the Euclidean distance between regions i and j and the fitted lambda parameter, $\lambda = 0.12 \text{ mm}^{-1}$ (EDR). Then, as in work by Pang et al. (5), we created a binary adjacency matrix where nodes i and j are retained and binarized only if the weight strength surpasses randomly distributed distribution of the weights. This option results in a binary adjacency matrix whereby $C_{ij} = 1$ if i and j are above randomly distributed distribution of the weights and $C_{ij} = 0$ if i and j are below the randomly distributed distribution of the weights. The choice of this approach was motivated to stay consistent with previous work by Pang et al. (5) in order for the results to be directly comparable.

EDR continuous. For the EDR continuous, we similarly use the EDR with the same parameters to define the weight of a given edge between vertices i and j using the EDR with $\lambda = 0.12 \text{ mm}^{-1}$. Unlike the thresholding in EDR binary [applied in work of Pang et al. (5)] where connections are retained and binarized if they surpass connection weights from a randomly derived distribution, here all the connections and their weights are kept. This option results in a weighted adjacency matrix whereby $W_{ij} = Ae^{-\lambda r(i,j)}$. Furthermore, we argue in this paper that this detailed explanation between EDR binary and EDR continuous adjacency matrices is warranted as it zeroes in on what is an appropriate comparison between graph Laplacian, and continuous Laplace-Beltrami analysis and we motivate future comparative research in this direction.

Geometry. The geometric modes were calculated using the Laplace-Beltrami operator (LBO) on the cortical mesh. We used the publicly available version from previously published work by Pang et al. which can be downloaded from <https://osf.io/xczmp/> in "fsLR_32k_midthickness-lh_emode_200".txt file (5). In brief, the LBO is in general defined as follows:

$$\Delta = \frac{1}{W} \sum_{i,j} \frac{\delta}{\delta x_i} (g^{ij} W \frac{\delta}{\delta x_j}),$$

with g^{ij} being the inverse of the inner product metric tensor $g_{ij} = \langle \frac{\delta}{\delta x_i}, \frac{\delta}{\delta x_j} \rangle$, $W = \det(G)$ and $G = (g_{ij})$. The solution of the eigenvalue problem was implemented in a python package LaPy using the cubic finite element method (36).

For further details, consult work by Pang et al. (5). Although not explicitly stated, the derivation leverages an exponential kernel that is reminiscent of the EDR.

EDR+LR. Previous research has shown that human as well as nonprimate anatomy is characterized by a relatively small proportion of LR outliers to the EDR (10, 12). Therefore, for the EDR continuous adjacency matrix, we wanted to implement a version where these LR exceptions are taken into account. Using the structural connectivity matrix, we computed the binned distribution (400 bins) as a function of Euclidean distance. We defined connectivity exceptions as three SD above the mean for a given distance bin that are longer than 40 mm (SI Appendix, Fig. S2). To derive the EDR+LR connectivity matrix, we combine the EDR continuous with LR exceptions to the EDR. Moreover, we also created a shuffled EDR+LR where the locations of the LR were randomly assigned in the connectivity matrix (SI Appendix, Fig. S4).

EDR+LR relationship to connectome harmonics. Combining short-range and LR connectivity can be performed in many ways. Indeed, our previous work on connectome harmonics has defined the anatomical connectivity in terms of short-range, nearest-neighbor connections on the cortical surface, combined together with LR connections, derived from the diffusion MRI in terms of the connectome (4). In this light, here, we derive the short-range connections in a more principled way through the "EDR continuous" while accounting for the LR connections in terms of the exceptions to the EDR as stated above. Furthermore, we avoid binarization of the adjacency matrix for the calculation of the Laplacian as it has shown to retain important information in the reconstruction of both spontaneous and task-evoked fMRI from our results on binary and continuous EDR brain modes.

Laplacian decomposition. Having derived the EDR+LR, EDR binary, and EDR continuous adjacency matrix, we calculated the normalized graph Laplacian as

$$L^{\text{norm}} = D^{-1/2} L D^{-1/2},$$

with $L = D - A$, where D is the diagonal degree matrix defined as $D = \sum_{j=1}^n A(i, j)$. Finally, the harmonic modes were computed as eigenvectors of the following eigenvalue problem

$$\Delta_A \psi_k(x_i) = \lambda \psi_k(x_i), \forall x_i \in v,$$

with $\lambda_k, k \in 1, \dots, n$ are the eigenvalues of Δ_A and ψ_k is the k th harmonic mode. We report visually the harmonic modes for EDR+LR, geometry, EDR continuous, and EDR binary rendered on the brain (SI Appendix, Fig. S1).

Decomposition of brain activity with harmonic modes. The spatiotemporal spontaneous fMRI recording and the activation maps of task-based fMRI can be represented as a weighted contribution of the harmonic modes as follows:

$$F(x, t) = \sum_{k=1}^N a_k(t) \psi_k(x),$$

where F is the spatiotemporal time recordings for each subjects with dimension $32,492 \times 1,200$ (x, t), $a_k(t)$ has dimension $1 \times 1,200$ and is the contribution of k th harmonic to the F timecourse at time t . The same rationale applies to the task-based fMRI except of the contributions being independent of time, i.e., $a_k(t) \rightarrow a_k$. Both in spontaneous and task-based fMRI, the contributions are computed as the inner product between the spatial patterns and harmonic modes

$$a_k(t) = \langle \langle F(x, t), \psi_k(x) \rangle \rangle.$$

Reconstruction error. To compare both the spontaneous and task-based empirical fMRI data with the reconstructed data with a subset of harmonic modes, we first parcellated the data to Glasser360 parcellation (we focused on the left hemisphere resulting in 180 nodes). For the spontaneous fMRI, we calculated the interregional FC (FC -180 x 180) and focused on the most salient features by reconstructing the LR FC derived as a subset of connections with high-correlation values (>0.5 correlation) and a long Euclidean distance (>40 mm). Then, we calculated the reconstruction error as the mse distance between the empirical and reconstructed LR FC. For the task-based fMRI, we calculated the reconstruction error as the mse distance between the empirical and reconstructed task-activation maps. Finally, for the behavioral analysis of SI Appendix, Figs. S6-S8, we correlated the reconstruction (for 200 modes) of spontaneous and task-evoked activity with fluid intelligence of participants in terms of three variables in the HCP data, namely 1) the number of correct responses in the PMAT24 A test and 2) processing speed in terms of Pattern Completion Processing Speed (CardSort_UnAdj and ProcSpeed_UnAdj) (37).

Data, Materials, and Software Availability. Code data have been deposited in BrainEigenmodes_EDRLR (https://github.com/jvohryzek/BrainEigenmodes_EDRLR). Previously published data were used for this work (32).

ACKNOWLEDGMENTS. Jakub Vohryzek is supported by EU H2020 FET Proactive project Neurotwin grant Agreement No. 101017716. Yonatan Sanz-Perl is supported by "ERDF A way of making Europe," ERDF, EU, Project NEurological MEchanismS of Injury, and Sleep-like cellular dynamics (NEMESIS; ref. 101071900) funded by the EU ERC Synergy Horizon Europe. Morten L. Kringelbach is supported by the European Research Council Consolidator Grant: CAREGIVING (615539), Pettit Foundation, Carlsberg Foundation, and Center for Music in the Brain, funded by the Danish National Research Foundation (DNRF117). Gustavo Deco is supported by the Spanish Research Project PSI2016-75688-P (Agencia

Estat de Investigación/Fondo Europeo de Desarrollo Regional, European Union); by the European Union's Horizon 2020 Research and Innovation Programme under Grant Agreements 720270 (Human Brain Project [HBP] SGA1) and 785907 (HBP SGA2); and by the Catalan Agency for Management of University and Research Grants Programme 2017 SGR 1545.

Author affiliations: ^aCentre for Brain and Cognition, Computational Neuroscience Group, Department of Information and Communication Technologies, Universitat Pompeu Fabra, Barcelona 08018, Spain; ^bDepartment of Psychiatry, Centre for Eudaimonia and Human Flourishing, Linacre College, University of Oxford, Oxford OX3 9BX, United Kingdom; ^cDepartment of Psychiatry, University of Oxford, Oxford OX3 7JX, United Kingdom; ^dDepartment of Clinical Medicine, Centre for Music in the Brain, Aarhus University, Aarhus 8000, Denmark; and ^eInstitució Catalana de la Recerca i Estudis Avançats, Barcelona 08010, Spain

1. E. Bullmore, O. Sporns, Complex brain networks: Graph theoretical analysis of structural and functional systems. *Nat. Rev. Neurosci.* **10**, 186–198 (2009).
2. M. Breakspear, Dynamic models of large-scale brain activity. *Nat. Neurosci.* **20**, 340–352 (2017).
3. M. G. Preti, D. Van De Ville, Decoupling of brain function from structure reveals regional behavioral specialization in humans. *Nat. Commun.* **10**, 4747 (2019).
4. S. Atasoy, I. Donnelly, J. Pearson, Human brain networks function in connectome-specific harmonic waves. *Nat. Commun.* **7**, 10340 (2016).
5. J. C. Pang *et al.*, Geometric constraints on human brain function. *Nature* **618**, 566–574 (2023).
6. M. Ercey-Ravasz *et al.*, A predictive network model of cerebral cortical connectivity based on a distance rule. *Neuron* **80**, 184–197 (2013).
7. M. Belkin, P. Niyogi, Laplacian eigenmaps for dimensionality reduction and data representation. *Neural Comput.* **15**, 1373–1396 (2003).
8. J. Faskowitz *et al.*, Commentary on Pang *et al.* (2023). *Nature*. bioRxiv [Preprint] (2023). <https://doi.org/10.1101/2023.07.20.549785> (Accessed 22 July 2023).
9. J. C. Pang *et al.*, Reply to: Commentary on Pang *et al.* (2023). *Nature*. bioRxiv [Preprint] (2023). <https://doi.org/10.1101/2023.10.06.560797> (Accessed 9 October 2023).
10. N. T. Markov *et al.*, The role of long-range connections on the specificity of the macaque interareal cortical network. *Proc. Natl. Acad. Sci. U.S.A.* **110**, 5187–5192 (2013).
11. N. T. Markov *et al.*, Cortical high-density counterstream architectures. *Science* **342**, 1238406 (2013).
12. G. Deco *et al.*, Rare long-range cortical connections enhance human information processing. *Curr. Biol.* **31**, 1–13 (2021).
13. S. Atasoy, G. Deco, M. L. Kringelbach, J. Pearson, Harmonic brain modes: A unifying framework for linking space and time in brain dynamics. *Neuroscientist* **24**, 277–293 (2018).
14. M. D. Fox *et al.*, The human brain is intrinsically organized into dynamic, anticorrelated functional networks. *Proc. Natl. Acad. Sci. U.S.A.* **102**, 9673–9678 (2005).
15. Y. Sanz Perl *et al.*, Whole-brain modelling of low-dimensional manifold modes reveals organising principle of brain dynamics. bioRxiv [Preprint] (2023). <https://doi.org/10.1101/2023.11.20.567824>.
16. J. Vohryzek *et al.*, The flattening of spacetime hierarchy of the N, N-dimethyltryptamine brain state is characterized by harmonic decomposition of spacetime (HADES) framework. *Natl. Sci. Rev.* **11**, nwae124 (2024).
17. F. E. Turkheimer *et al.*, A complex systems perspective on neuroimaging studies of behavior and its disorders. *Neuroscientist* **28**, 382–399 (2022).
18. M. G. Preti, T. A. Bolton, D. Van De Ville, The dynamic functional connectome: State-of-the-art and perspectives. *NeuroImage* **160**, 41–54 (2017).
19. J. Vohryzek, J. Cabral, P. Vuust, G. Deco, M. L. Kringelbach, Understanding brain states across spacetime informed by whole-brain modelling. *Philos. Trans. A, Math. Phys. Eng. Sci.* **380**, 20210247 (2022).
20. G. Northoff, S. Wainio-Theberge, K. Evers, Is temporo-spatial dynamics the "common currency" of brain and mind? In quest of "spatiotemporal neuroscience". *Phys. Life Rev.* **33**, 34–54 (2020).
21. G. Northoff, "From brain dynamics to the mind" in *From Brain Dynamics to the Mind: Spatiotemporal Neuroscience*, M. McManus, Ed. (Elsevier, 2024), pp. 1–661.
22. G. Deco, G. Tononi, M. Boly, M. L. Kringelbach, Rethinking segregation and integration: Contributions of whole-brain modelling. *Nat. Rev. Neurosci.* **16**, 430–439 (2015).
23. H. Jaeger, B. Noheda, W. G. Van Der Wiel, Toward a formal theory for computing machines made out of whatever physics offers. *Nat. Commun.* **14**, 4911 (2023).
24. S. Mansour *et al.*, Eigenmodes of the brain: Revisiting connectomics and geometry. bioRxiv [Preprint] (2018). <https://doi.org/10.1101/2024.04.16.589843> (Accessed 20 April 2024).
25. C. Reveley *et al.*, Superficial white matter fiber systems impede detection of long-range cortical connections in diffusion MR tractography. *Proc. Natl. Acad. Sci. U.S.A.* **112**, E2820–E2828 (2015).
26. C. J. Donahue *et al.*, Using diffusion tractography to predict cortical connection strength and distance: A quantitative comparison with tracers in the monkey. *J. Neurosci.* **36**, 6758–6770 (2016).
27. S. Horvát *et al.*, Spatial embedding and wiring cost constrain the functional layout of the cortical network of rodents and primates. *PLoS Biol.* **14**, e1002512 (2016).
28. L. Magrou *et al.*, The meso-connectomes of mouse, marmoset, and macaque: Network organization and the emergence of higher cognition. *Cereb. Cortex* **34**, bhae174 (2024).
29. J. Vohryzek *et al.*, Dynamic sensitivity analysis: Defining personalised strategies to drive brain state transitions via whole brain modelling. *Comput. Struct. Biotechnol. J.* **21**, 335–345 (2023).
30. A. Menardi *et al.*, Toward noninvasive brain stimulation 2.0 in Alzheimer's disease. *Ageing Res. Rev.* **75**, 101555 (2022).
31. D. M. Barch *et al.*, Function in the human connectome: Task-fMRI and individual differences in behavior. *NeuroImage* **80**, 169–189 (2013).
32. D. C. Van Essen *et al.*, The WU-minn human connectome project: An overview. *NeuroImage* **80**, 62–79 (2013).
33. M. W. Woolrich, T. E. Behrens, C. F. Beckmann, M. Jenkinson, S. M. Smith, Multilevel linear modelling for fMRI group analysis using Bayesian inference. *NeuroImage* **21**, 1732–1747 (2004).
34. Y. Tian, B. T. Yeo, V. Cropley, A. Zalesky, High-resolution connectomic fingerprints: Mapping neural identity and behavior. *NeuroImage* **229**, 117695 (2021).
35. J. D. Tournier *et al.*, MRtrix3: A fast, flexible and open software framework for medical image processing and visualisation. *NeuroImage* **202**, 116137 (2019).
36. M. Reuter, F.-E. Wolter, N. Peinecke, Laplace-Beltrami spectra as 'Shape-DNA' of surfaces and solids. *Comput. Aided Des.* **38**, 342–366 (2006).
37. P. Ritter, M. Schirner, A. R. McIntosh, V. K. Jirsa, The virtual brain integrates computational modeling and multimodal neuroimaging. *Brain Connect.* **3**, 121–145 (2013).